Ligand Charge Separation to Build Highly Stable Quasi-Isomer of MOF-74-Zn

Huajun Yang,[a] Fang Peng,[a] Candy Dang,[a] Yong Wang,[b] Dandan Hu,[b] Xiang Zhao,[b] Pingyun Feng,[b] and Xianhui Bu[a]

[a] College of Chemistry and Biochemistry, California State University, Long Beach, California 90840, United States

[b] Department of Chemistry, University of California, Riverside, California 92521, United States

Experimental Section:

Chemicals and Materials. Zinc nitrate hexahydrate ($Zn(NO_3)_2 \cdot 6H_2O$, 98%), 2-hydroxyterephthalic acid (H_3OBDC, >98%), N,N-dimethylformamide (DMF, 99.5%), N,N-dibutylformamide (DBF, >99%), and ethanol (EtOH, 99%), isopropanol (iPrOH, 99.5%), tetrapropylammonium hydroxide (TPAOH, 1.0 M solution in water) were all used without any further purification.

Synthesis of CPM-74 [$Zn_2(OH)(OBDC) \cdot 1.75H_2O \cdot$xGuest]: A mixture of $Zn(NO_3)_2 \cdot 6H_2O$ (30 mg, 0.1 mmol), H_3OBDC (9.1 mg, 0.05 mmol), DMF (2 g), DBF (0.5 g), iPrOH (0.5 g), water (0.5 g), and TPAOH (50 μL, 0.05 mmol) was stirred in a 15 mL scintillation vial for about one hour. After being heated in 120 ℃ oven for five days, pale-yellow rod-like crystals were obtained. Large-sized crystals can also be synthesized by reacting the mixture of $Zn(NO_3)_2 \cdot 6H_2O$ (60 mg, 0.2 mmol), H_3OBDC (18.2 mg, 0.1 mmol), DMF (2 g), DBF (0.5 g), iPrOH (0.5 g), and water (0.5 g) in 120 ℃ oven for five days. The phase purity was identified by powder X-ray diffraction. Based on TGA analysis (Figure S9 top), the guests in the pore account for around 20% of the total weight.

Synthesis of CPM-75 [$Zn_2(OH)(OBPDC) \cdot 2H_2O \cdot$xGuest]: A mixture of $Zn(NO_3)_2 \cdot 6H_2O$ (30 mg, 0.2 mmol), H_3OBPDC (13.0 mg, 0.1 mmol), DMF (2.5 g), EtOH (0.5 g), water (0.5 g), and TPAOH (50 μL, 0.05 mmol) was stirred in a 15 mL scintillation vial for one hour. After being heated in 120 ℃ oven for five days, pale-yellow rod-like crystals were obtained. The crystal can also be synthesized in the absence of TPAOH. The phase purity was identified by powder X-ray diffraction.

Synthesis of MOF-74: The synthesis and activation of MOF-74 followed the reported procedures.[1]

Single-Crystal X-ray Diffraction Characterization. The single-crystal X-ray diffraction measurements of **CPM-74-75** were performed on a Bruker diffractometer using graphite-monochromated MoKα (λ= 0.71073 Å) radiation at room temperature. Diffraction data were integrated and scaled by 'multi-scan' method with the Bruker APEX software. The structure was solved by intrinsic phasing which was embedded in 'APEX III' software and the refinement against all reflections of the compound was performed using 'APEX III'. All non-hydrogen framework atoms were refined anisotropically. The oxygen atoms from the solvent were refined isotropically. The hydrogen atoms on trimer oxygen were located from the Fourier electron density map and other hydrogen atoms were calculated. CCDC 1909876-1909877 contain the supplementary crystallographic data for this paper. These data are provided free of charge by the Cambridge Crystallographic Data Centre.

Powder X-ray Diffraction (PXRD) Characterization. Powder X-ray diffraction experiments were performed on a PANalytical X'Pert Pro MPD diffractometer, equipped with a linear X'Celerator detector, which was operating at 40 kV and 35 mA (Cu Kα radiation, λ = 1.5418 Å). The data collection was performed at room temperature in the range from 5° to 40° with a step size of ~0.008°. The simulated powder pattern was obtained from the single crystal data.

Thermogravimetric (TG) Measurement. A TA Instruments TGA Q500 thermal analyzer was used to measure the TG curve by heating the sample from 30 ℃ to 800 ℃ with heating rate of 5℃/min under nitrogen flow. The flow rate of the nitrogen gas was controlled at about 60 milliliters per minute.

Thermal Stability Tests for CPM-74, CPM-75, and MOF-74. Around 5 mg of samples were heated from room temperature to different temperatures with a heating rate of 5℃/min under nitrogen flow. The samples were kept at different temperatures for one hour and then were allowed to be cooled to room temperature naturally. The processed samples were then

subject to PXRD experiments.

Water Stability Tests for CPM-74, CPM-75, and MOF-74. In one batch**,** around 10 mg of samples were immersed in 10 mL of water at room temperature. The samples were dried in air and used for PXRD experiments. The pH value was adjusted by diluting either concentrated HCl solution or sodium hydroxide solution.

Gas Sorption Measurement. Gas sorption measurements were carried out on a Micromeritics ASAP 2020 PLUS Physisorption Analyzer. Prior to the measurement, the as-synthesized sample of **CPM-74** was purified by DMF and then refluxed in methanol or ethanol for 2 days. After the sample was transferred into the test tube, it was first degassed under room temperature for 3 hours and further dried at 300 ^{o}C for over 24 hours. It should be noted that different activation temperatures were tested and it was optimized to be 300 ^{o}C, which is probably due to the high-boiling-point DBF molecules in the pore. For **CPM-75**, the solvent-exchange process was performed in methanol for three days at room temperature. The solution was refreshed three times in one day. The sample was then activated at 200 ^{o}C for overnight. The H_2 sorption measurement was performed at 77 K. The CO_2 and CH_4 adsorption experiments were both performed at 273 K and 298 K. N_2 adsorption experiments were performed at 77 K, and 298 K respectively.

Isosteric Heat of Adsorption. The isosteric heats of adsorption for CO_2 were calculated using the isotherms at 273 K and 298 K, following the Clausius-Clapeyron equation. It was done with the calculation program embedded in the software of ASAP 2020 plus.

Selectivity by IAST. To evaluate the CO_2 capture performance, the selectivity was calculated by ideal adsorbed solution theory (IAST). Single-site Langmuir (SSL) model or dual-site Langmuir (DSL) model was first employed to fit the gas adsorption isotherms of **CPM-74** over the entire pressure range. DSL model can be written as:

$$N = N_A + N_B = \frac{N_{A,sat} k_A p}{1 + k_A p} + \frac{N_{B,sat} k_B p}{1 + k_B p},$$

Where N is the quantity adsorbed, p is the pressure of bulk gas at equilibrium with adsorbed phase, $N_{A,sat}$ and $N_{B,sat}$ are the saturation loadings for sites A and B, and k_A and k_B are the Langmuir parameters for sites A and B, respectively. The parameters of $N_{A,sat}$, $N_{B,sat}$, k_A, and k_B were simplified as A, B, C, D in the fitting process by Origin software. The R factors for all the fitting are higher than 99.9%.

The detailed methodology for calculating the amount of A and B adsorption from a mixture by IAST is described elsewhere.[2] The adsorption selectivity is finally defined as:

$$Selectivity = \frac{q_A / q_B}{p_A / p_B}$$

where q_i (i = A or B) is the uptake quantity and p_i is the partial pressure of component i.

DFT Calculations. The models for Zn-containing clusters were cleaved from the unit cell of MOF-74 and CPM-74, respectively. The dangling bonds were saturated by H. The DFT (DFT-D2) calculations were performed to describe the interaction between the clusters and CO_2 molecules using DMol^3 module that was implemented in Materials Studio.[3-5] The Perdew–Burke–Ernzerhof (PBE) exchange-correlation potential combined with the double numerical basis set containing polarization function (DNP) was employed in the calculations. Core electrons were used to set the type of core treatment. The convergence threshold parameters for the optimization were 10^{-5} Ha (energy), 2×10^{-3} Ha/Å (gradient), and 5×10^{-3} Å (displacement), respectively.

The binding energy (BE) between the CO_2 molecules and MOFs was calculated as follows:

$$\Delta E = E_{\mathrm{MOFs-CO2}} - E_{\mathrm{MOFs}} - E_{\mathrm{CO2}} \qquad (1)$$

where E represents the energy of the system after geometry relaxation, $E_{\mathrm{MOFs-CO2}}$ is the total

energy of the MOFs and CO_2, E_{MOFs} and E_{CO2} are the energies of the isolated MOFs and CO_2 molecule, respectively.

Table S1. Comparison of the density of metal sites between MOF-74-Zn and CPM-74

Compounds	Formula	d_G (mmol/g)	d_V (mmol/cm^3)
MOF-74-Zn	$Zn_2C_8H_2O_6$	6.16	7.50
CPM-74	$Zn_2C_8H_4O_6$	6.12	7.86

d_G: gravimetric density of metal sites; d_V: volumetric density of metal sites.

Table S2. Crystal data and structure refinement parameters for Rod-Packing MOFs in CPM series $Zn_2(OH)(OBPDC)$

Compound	**CPM-74**	**CPM-75**
Structural formula	$Zn_2(OH)(OBDC)\cdot 1.75H_2O$	$Zn_2(OH)(OBPDC)\cdot 2H_2O$
Crystal system	Hexagonal	Orthorhombic
Space group	$P6_122$	*Fddd*
Z	12	32
a (Å)	22.026(4)	11.987(3)
b (Å)	22.026(4)	39.230(8)
c (Å)	12.068(2)	47.618(11)
α (deg.)	90	90
β (deg.)	90	90
γ (deg.)	120	90
V ($Å^3$)	5071 (2)	22393(8)
Completeness	99.8%	100.0%
Independent reflections	3889 (R_{int}=0.0356)	5108 (R_{int}=0.0537)
GOF on F^2	1.233	1.115
R_1, wR_2 ($I>2\sigma(I)$)	0.0396, 0.1329	0.0695, 0.2016
R_1, wR_2 (all data)	0.0440, 0.1358	0.1059, 0.2291
Largest diff. peak and hole	0.839, -0.677	1.781, -0.721

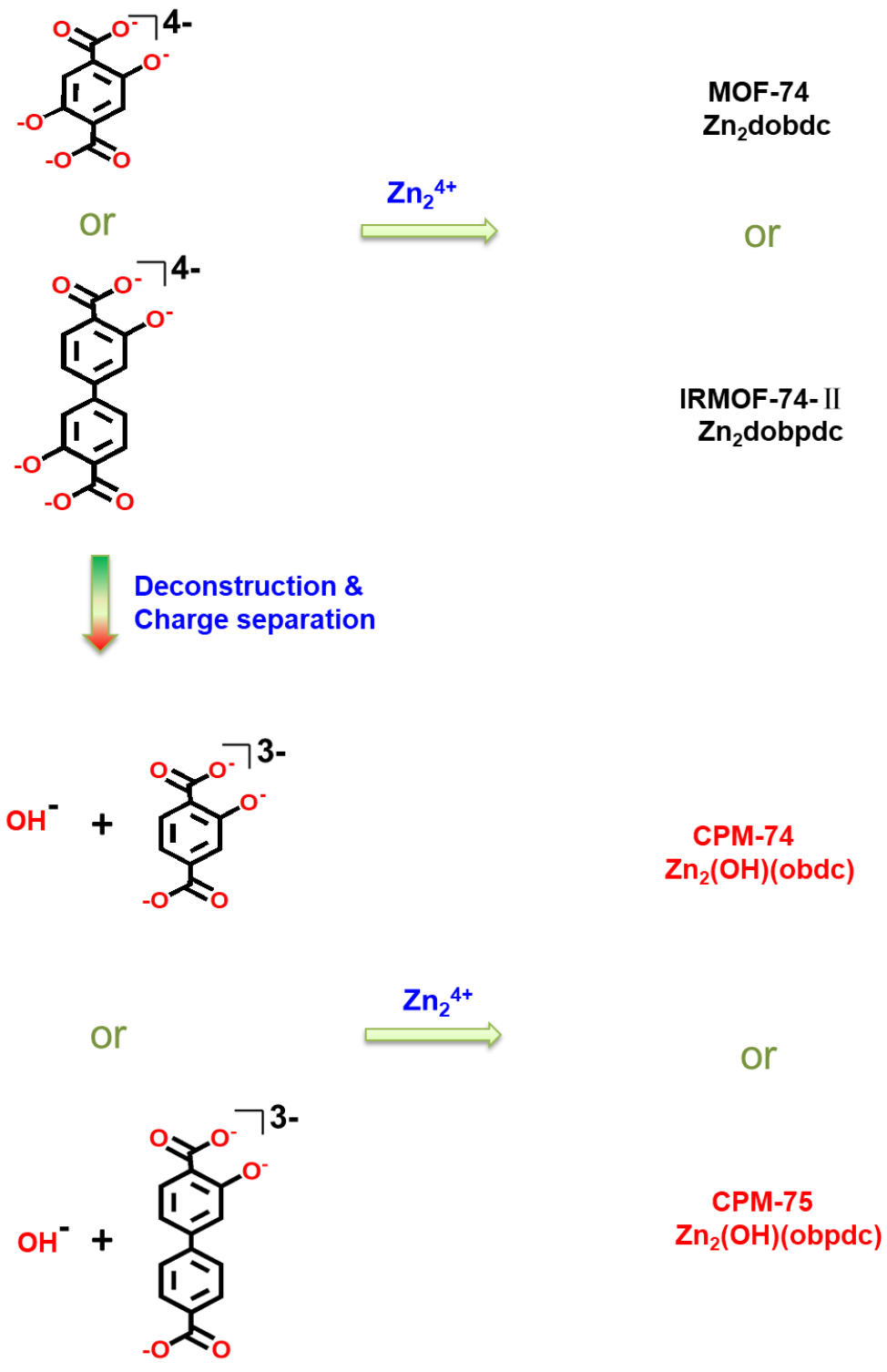

Scheme S1. Schematic illustration of ligand charge separation that leads to the discovery of CPM-74 and CPM-75.

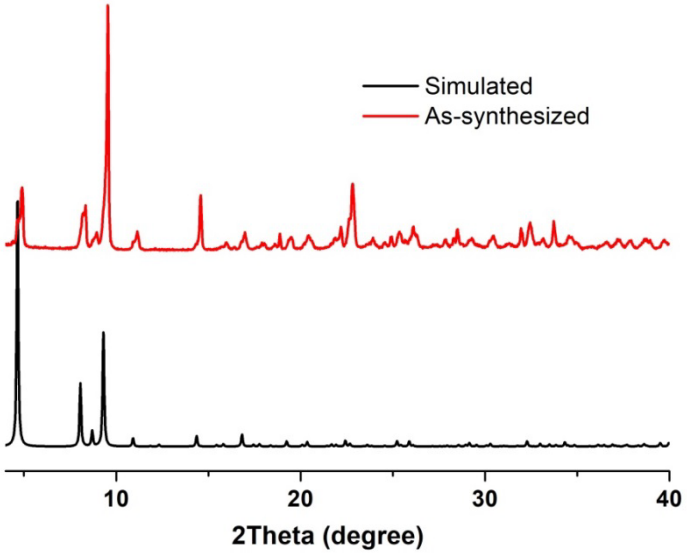

Figure S1. PXRD patterns of the as-synthesized and simulated **CPM-74**.

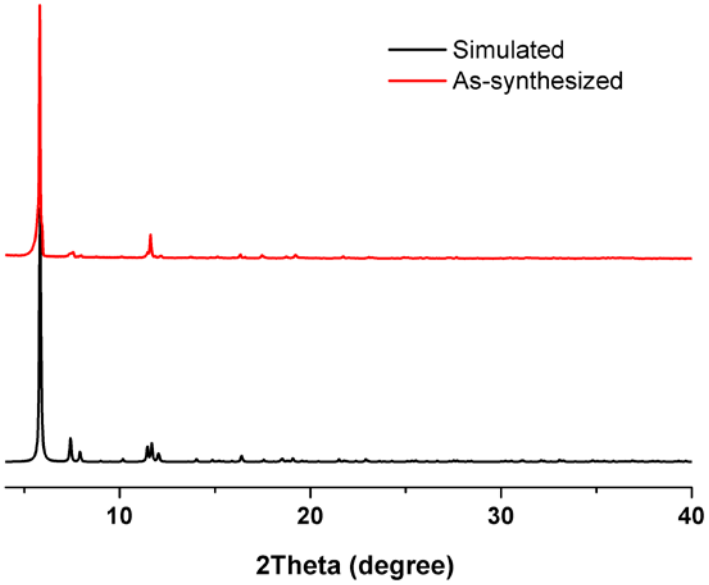

Figure S2. PXRD patterns of the as-synthesized and simulated **CPM-75**.

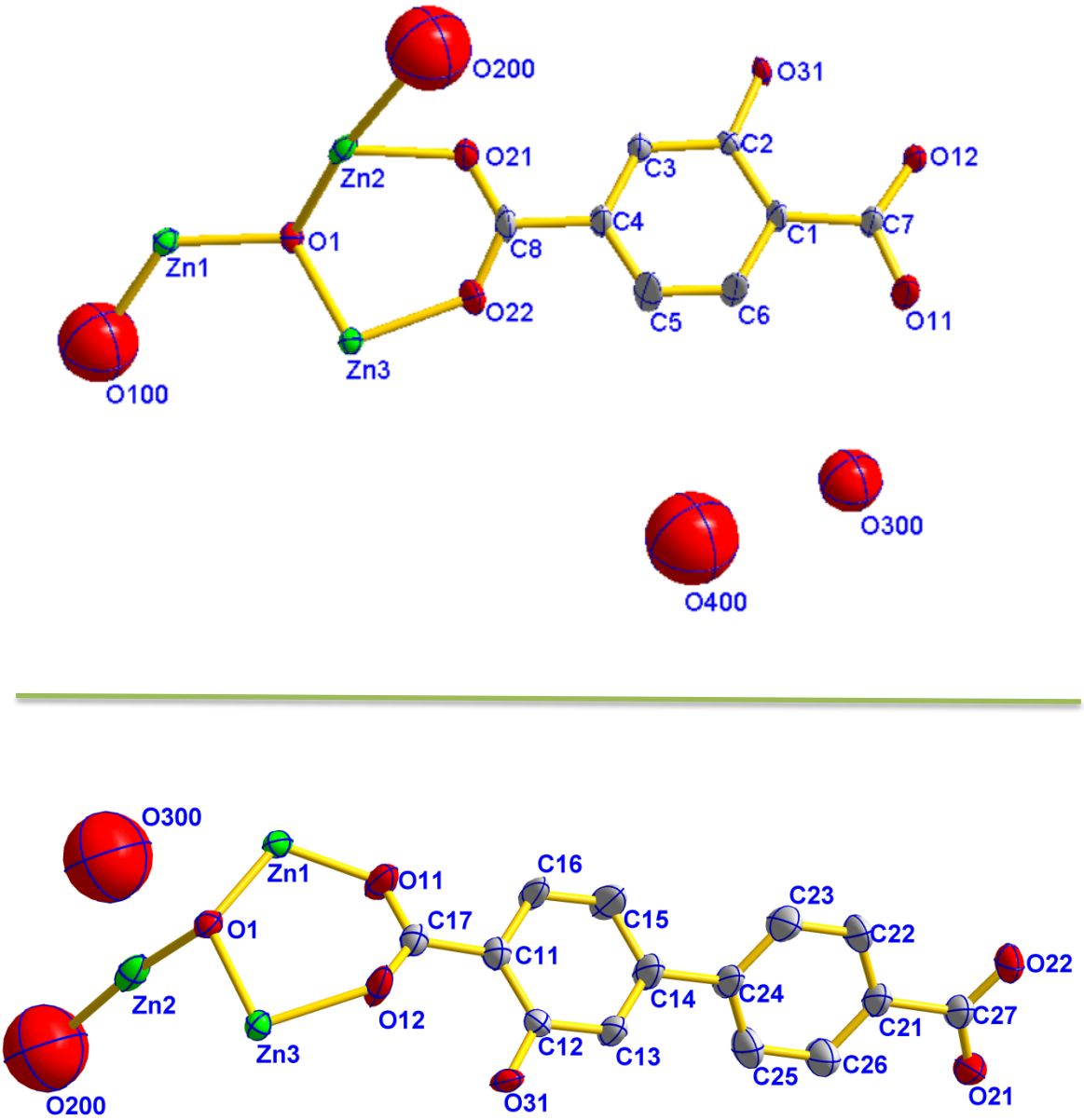

Figure S3. ORTEP drawing of the asymmetric unit of **CPM-74** (top) **and CPM-75** (bottom) with 50% probability (Green: Zn; Red: Oxygen; Gray: Carbon. Hydrogen atoms are omitted for clarity).

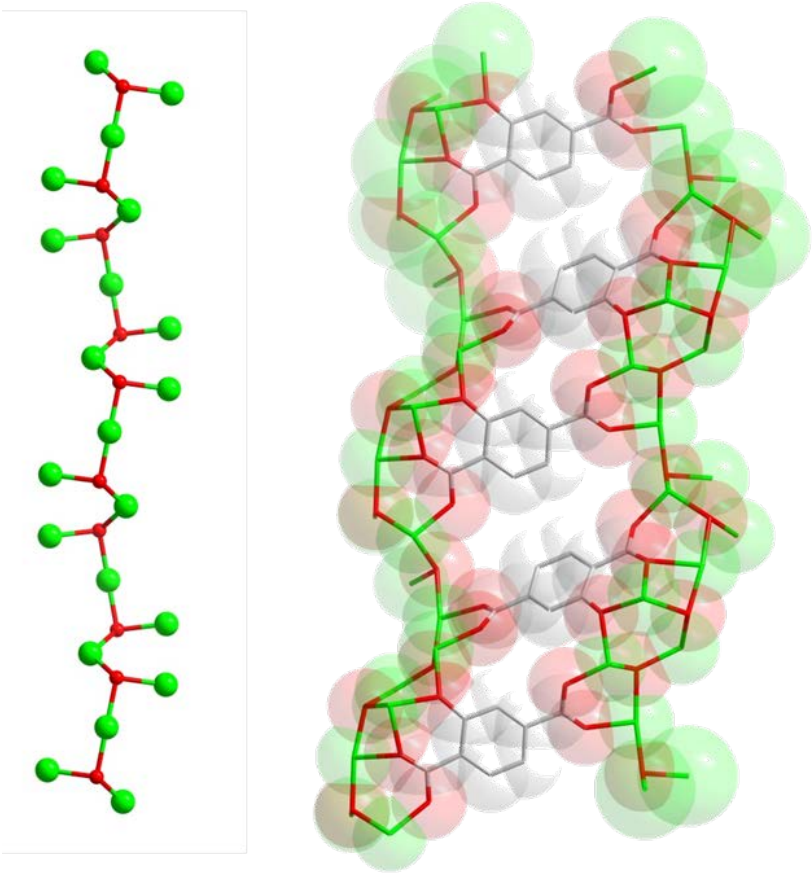

Figure S4. Core of the rod and the linkage between adjacent rods in **CPM-74.**

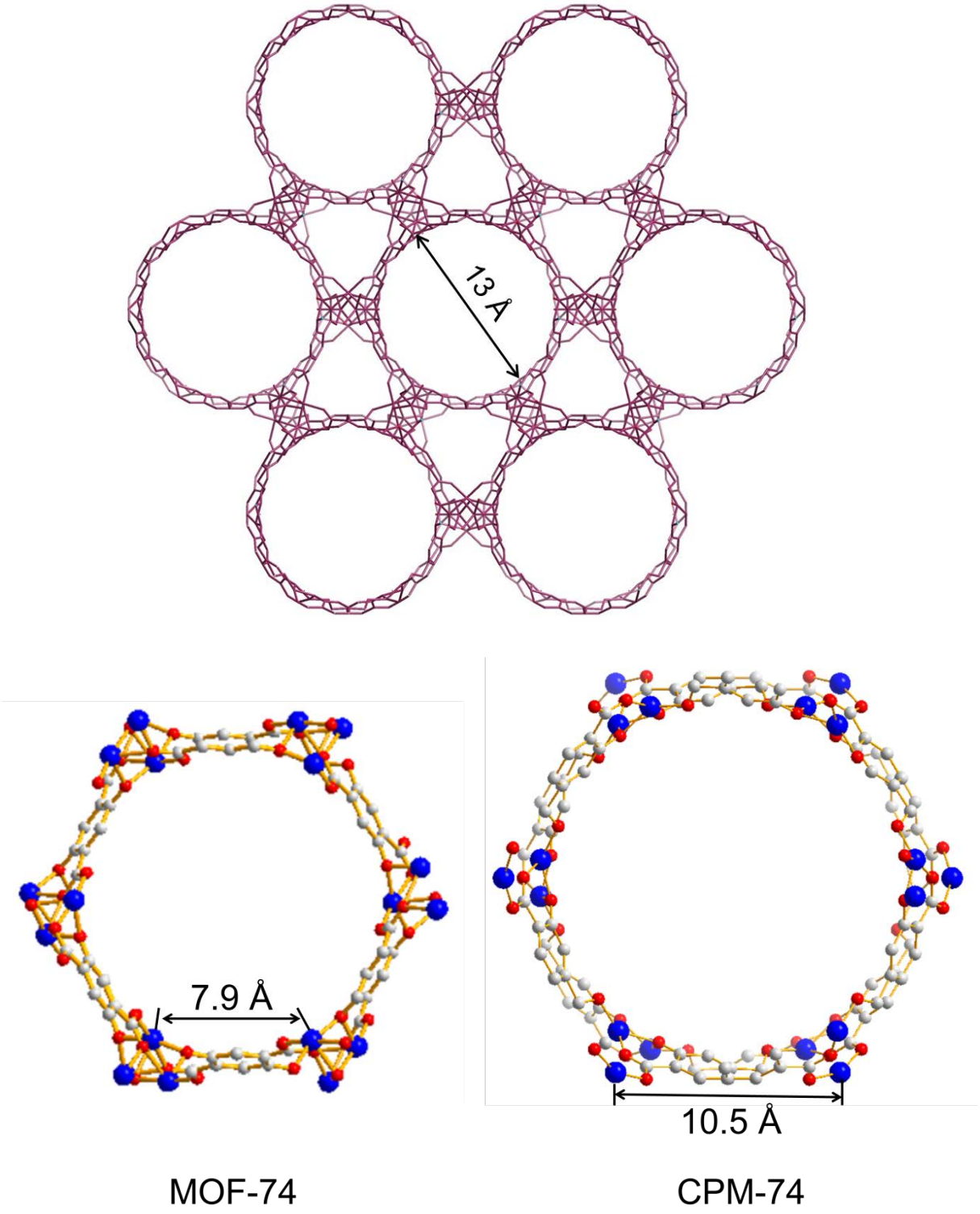

Figure S5. Wires mode of the architecture of **CPM-74** showing the hexagonal channel around 1.3 nm (top)**.** Comparisons of distances between the adjacent open metal sites in adjacent rod of MOF-74 and CPM-74

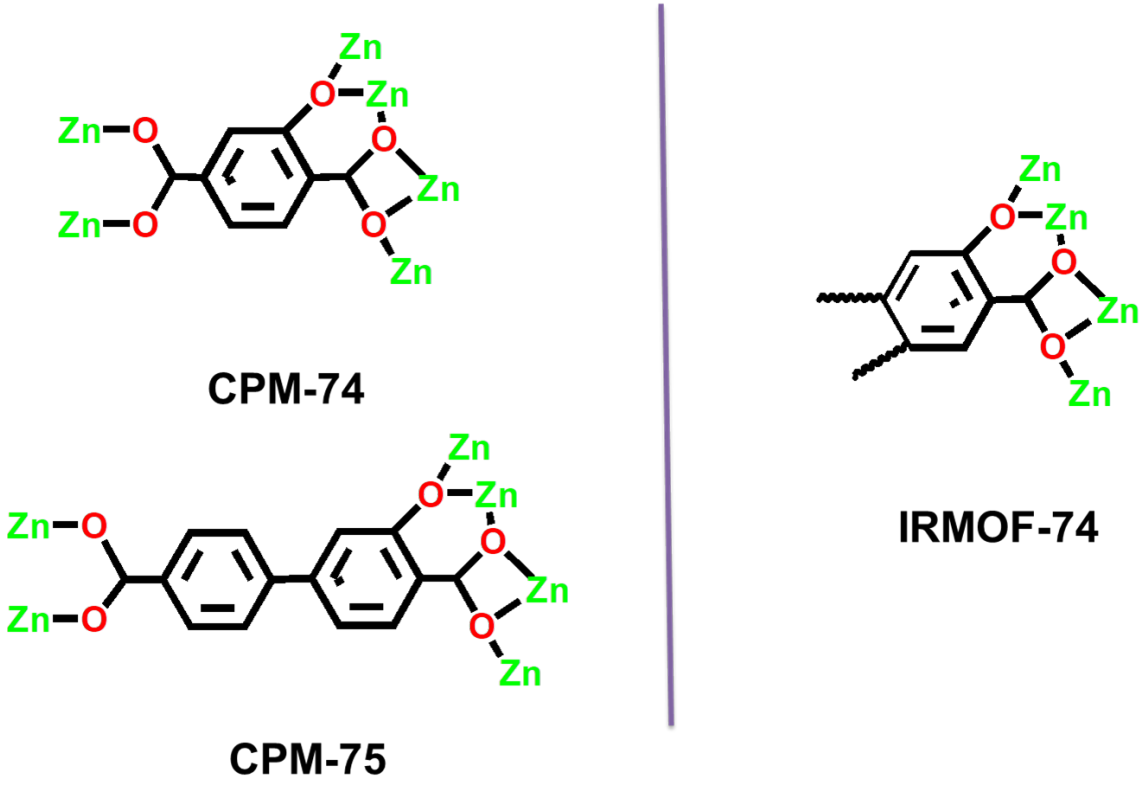

Figure S6. Comparison of coordination mode of H_3OBDC/H_3OBPDC ligand in **CPM-74, 75** with that of IRMOF-74s. Note: Considering that both sides of the ligands in IRMOF-74 have the same bonding mode, only one side is shown for clarity.

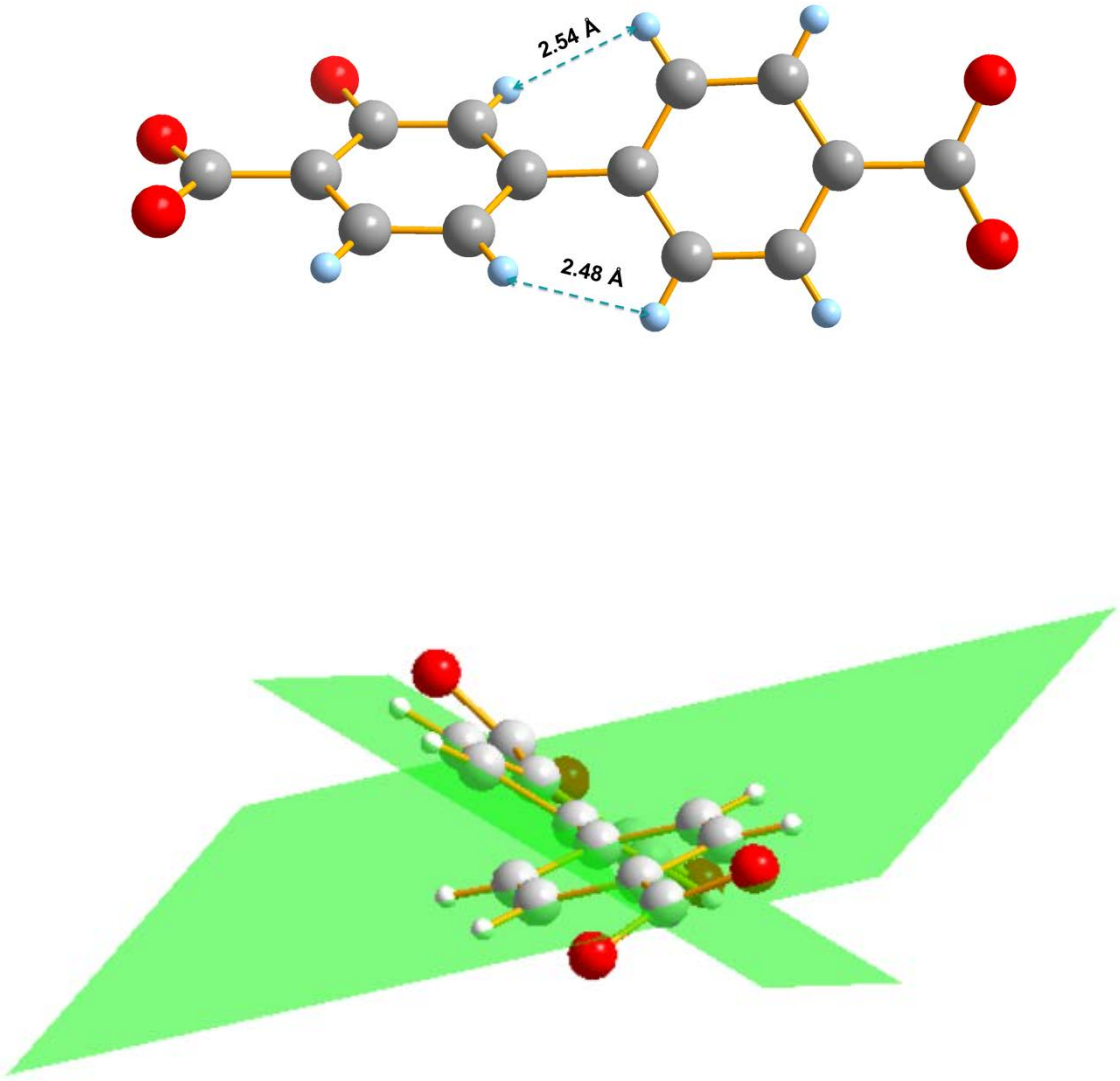

Figure S7. The geometric configuration of $OBPDC^{3-}$ in **CPM-75** showing the distances between the hydrogen atoms from the adjacent benzene rings. The angle between the planes defined by the adjacent benzene ring is 47.545^{o}.

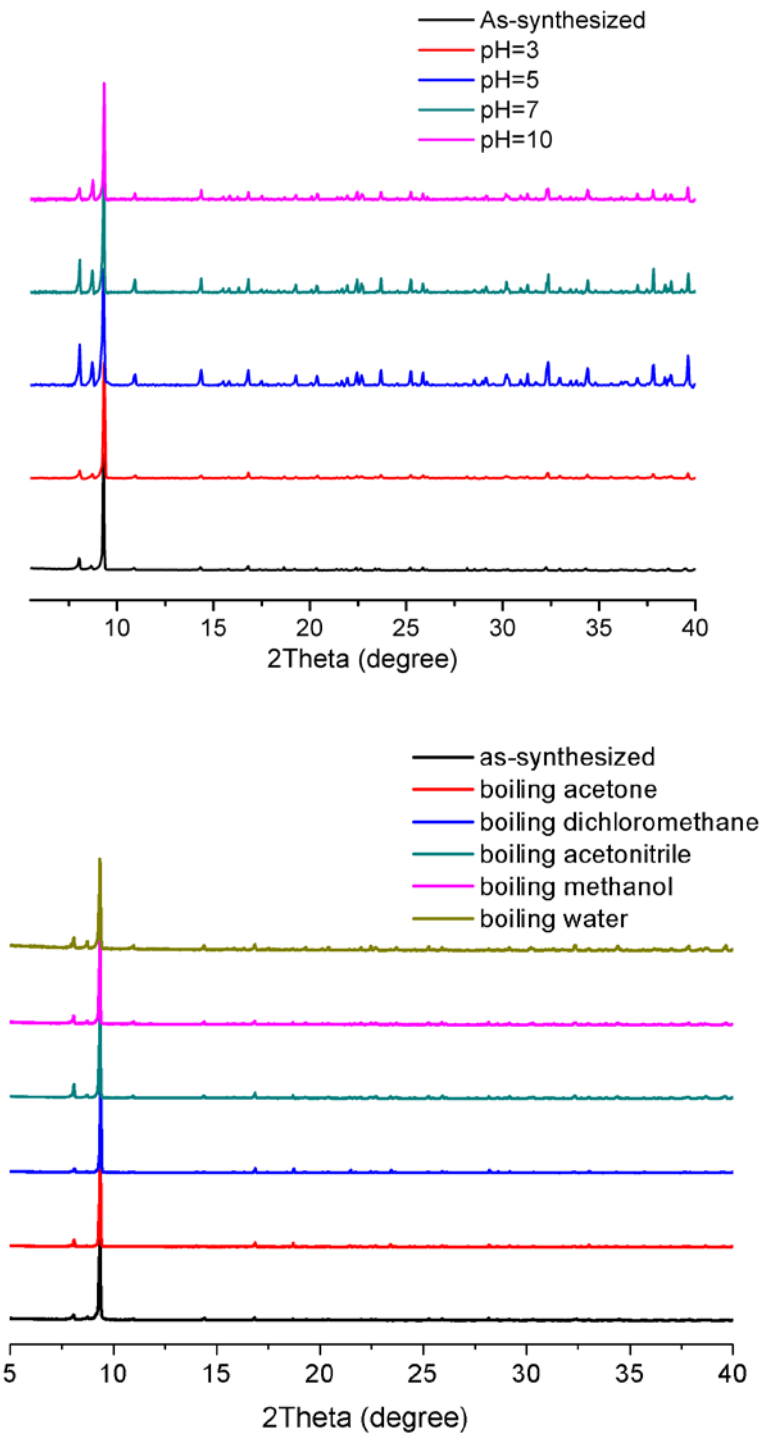

Figure S8. Comparison of PXRD patterns of **CPM-74** after immersing water solution for 24h with different pH (top); Comparison of PXRD patterns of **CPM-74** after immersing in boiling organic solvents and water for 1 hour (bottom).

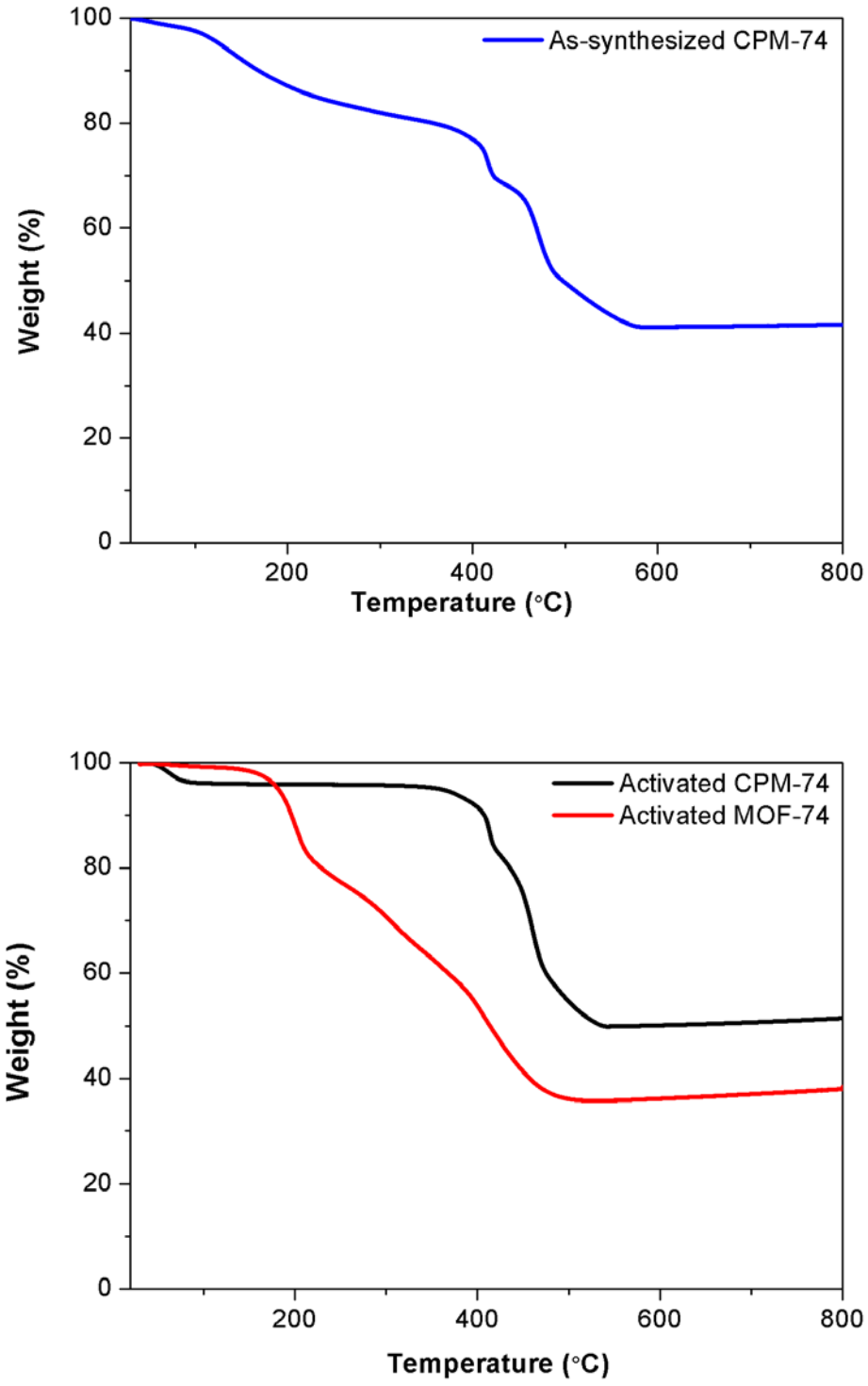

Figure S9. TGA trace of as-synthesized CPM-74 (top) and comparisons of TGA traces between activated **CPM-74** and activated MOF-74 (bottom).

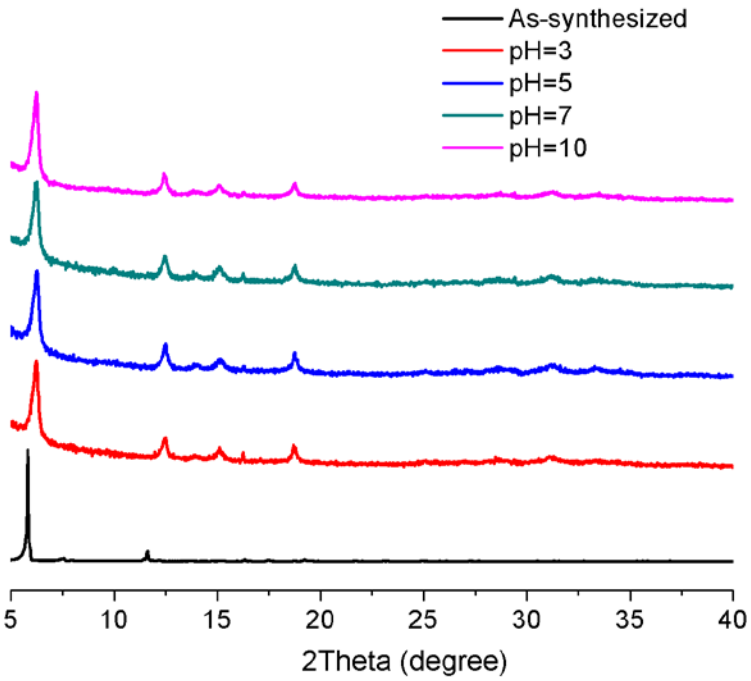

Figure S10. Comparison of PXRD patterns of **CPM-75** after immersing water solution for 24 hours with different pH.

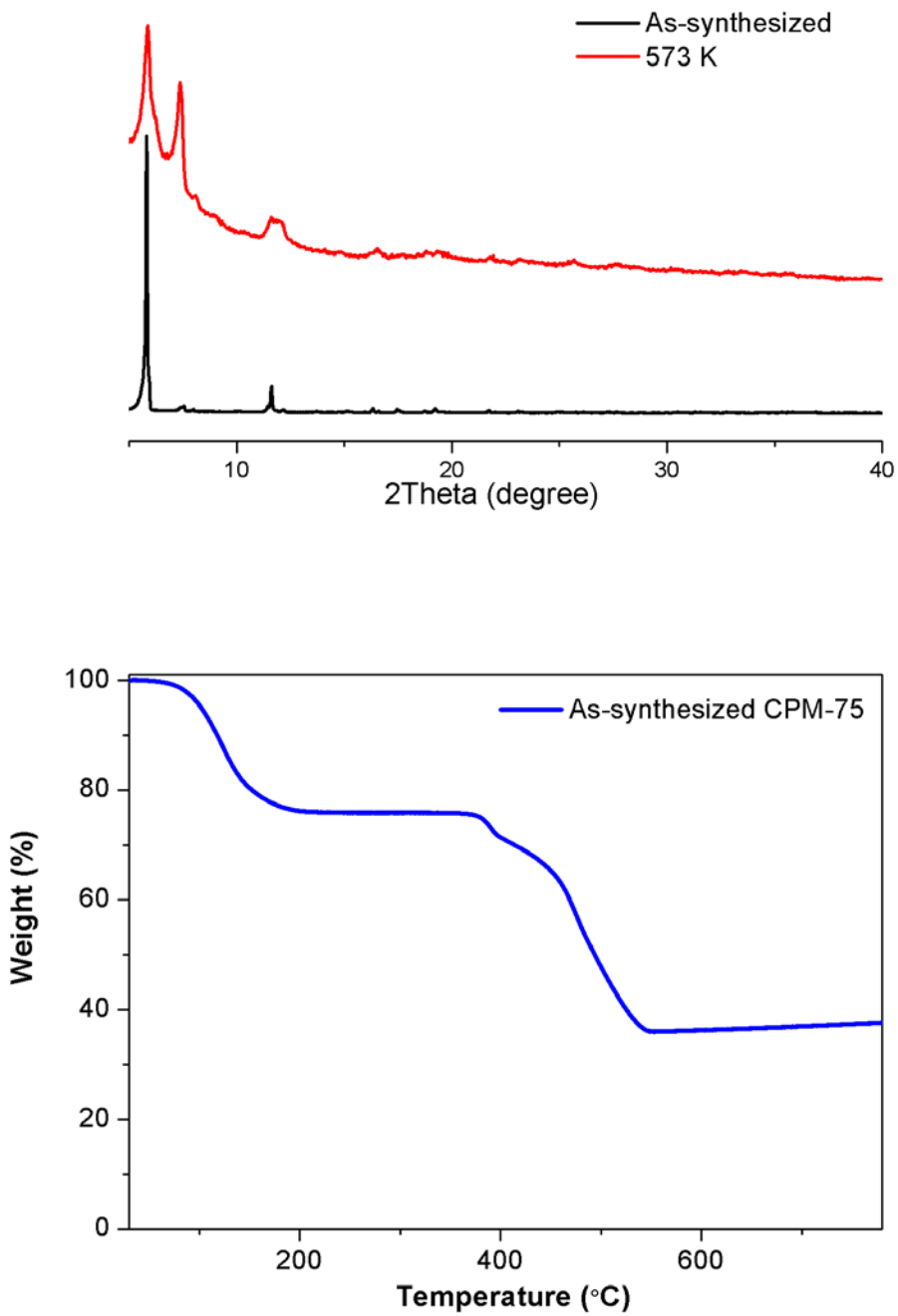

Figure S11. PXRD comparisons of as-synthesized and thermal-treated (573 K or 300 ^{o}C) **CPM-75** (top) and TGA trace of as-synthesized **CPM-75** (bottom).

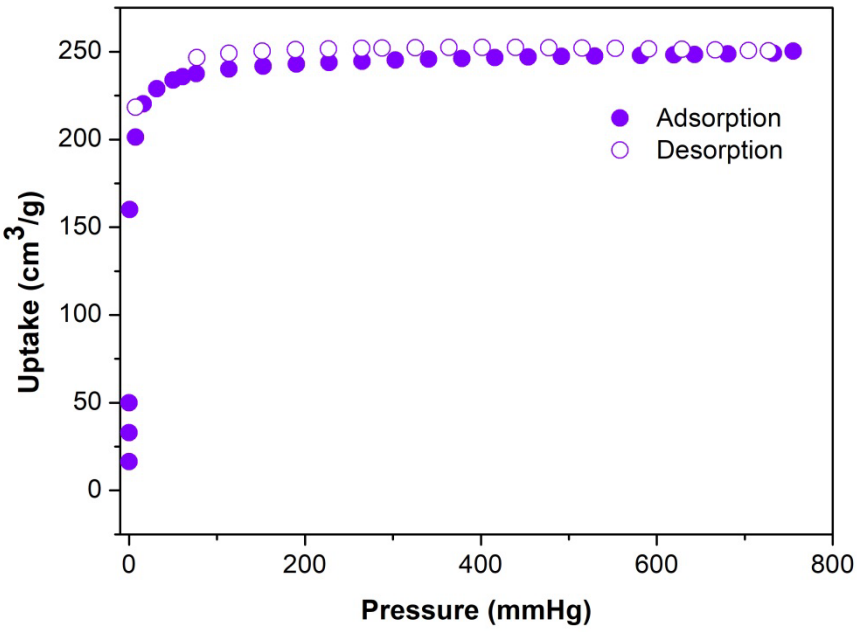

Figure S12. N_2 adsorption of **CPM-74** at 77 K.

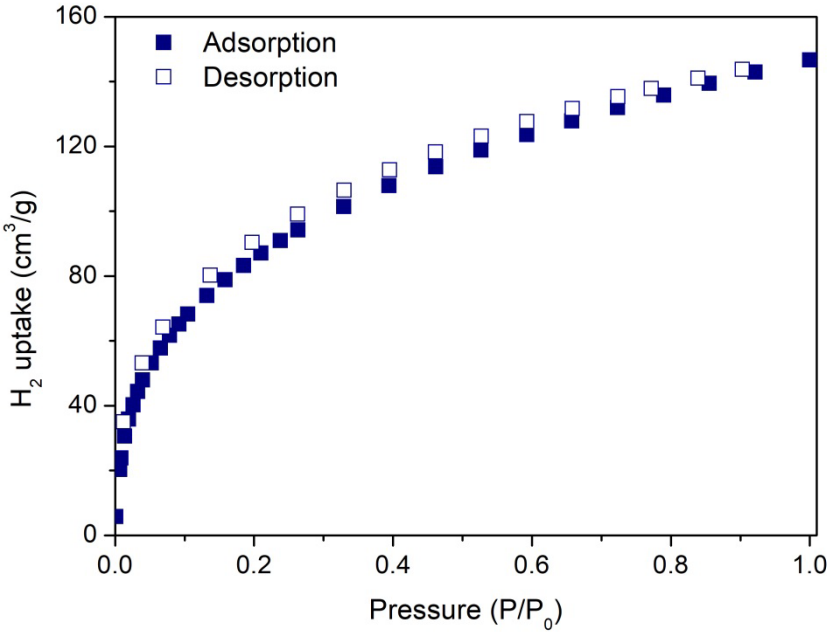

Figure S13. H_2 adsorption of CPM-74 at 77 K.

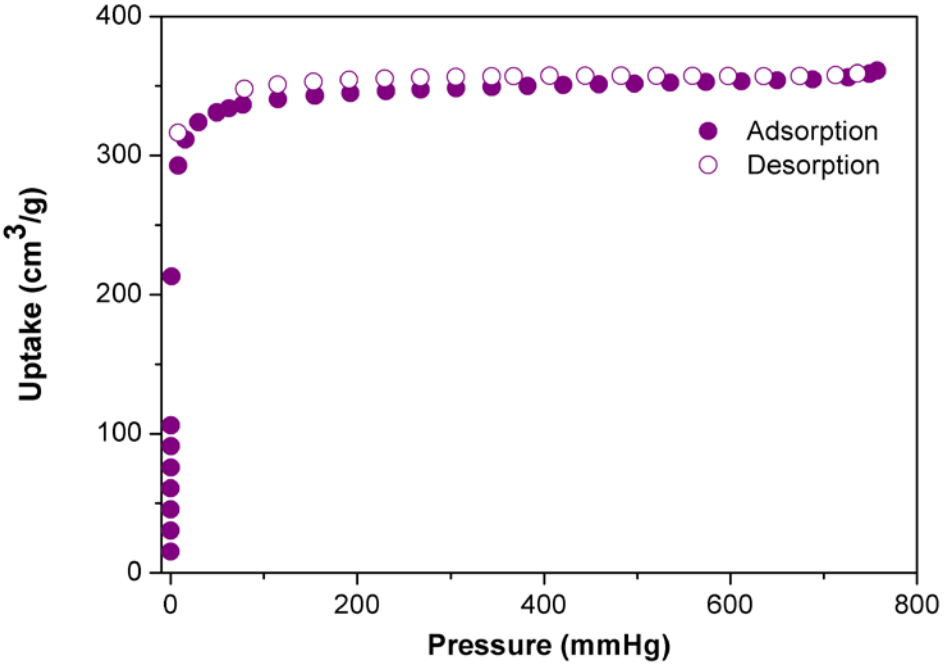

Figure S14. N_2 adsorption of **CPM-75** at 77 K.

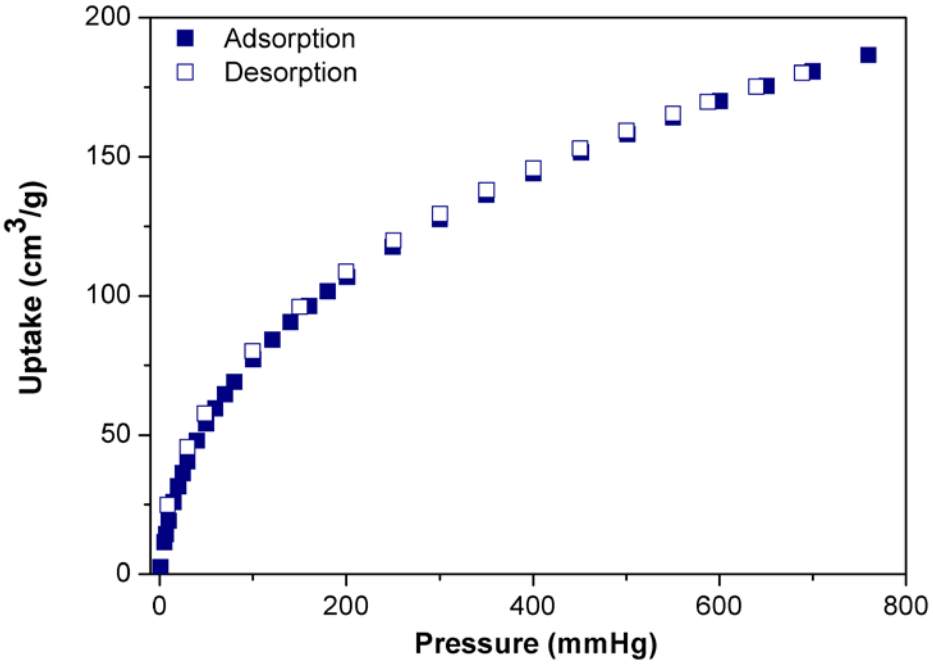

Figure S15. H_2 adsorption of **CPM-75** at 77 K.

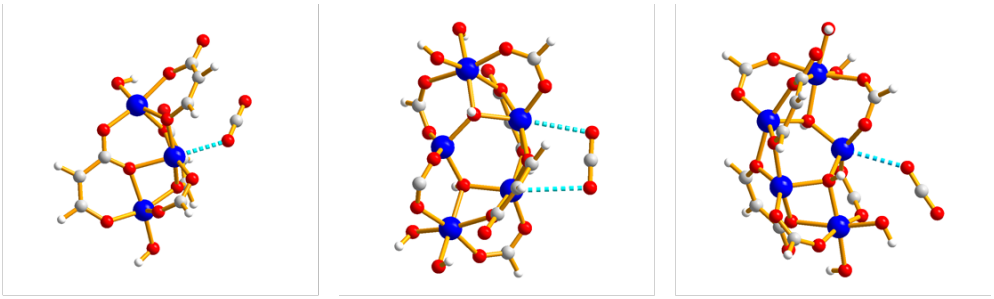

	MOF-74-Zn	CPM-74-Zn2	CPM-74-Zn1
Binding Energy	24.5 kJ/mol	12.2 kJ/mol	31.3 kJ/mol

Figure S16. DFT calculations on CO_2 binding energy in MOF-74 and **CPM-74**.

Figure S16 shows the most stable adsorption configurations for CO_2 adsorption over the Zn open metal sits of MOF-74 and **CPM-74**. The binding energy for MOF-74Zn is calculated to be −24.5 kJ/mol. For **CPM-74**, there are two possible binding sites including Zn1 and two adjacent Zn2 for cooperative bonding. The calculated binding energies for these two sites are 31.3 and 12.2 kJ/mol, respectively. Interestingly, for CO_2 binding on Zn1 in **CPM-74,** DFT optimization finds that the CO_2 is slight bent (175.9^o) towards the O in the carboxyl group bonding to Zn3, indicating a possible synergetic effect, which thereby contributes to the higher binding energy.

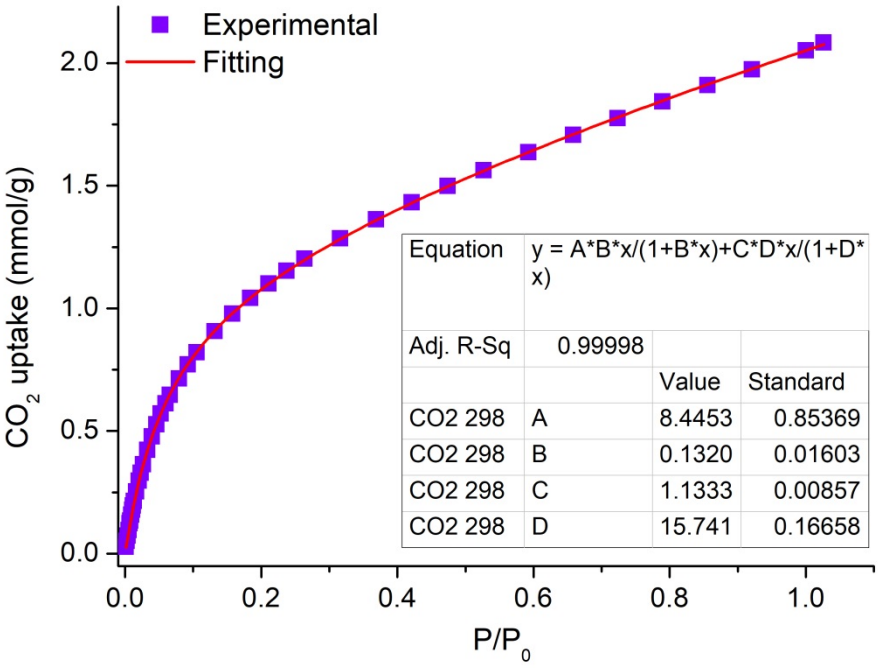

Figure S17. Dual-site Langmuir fitting of CO_2 adsorption of **CPM-74** at 298 K.

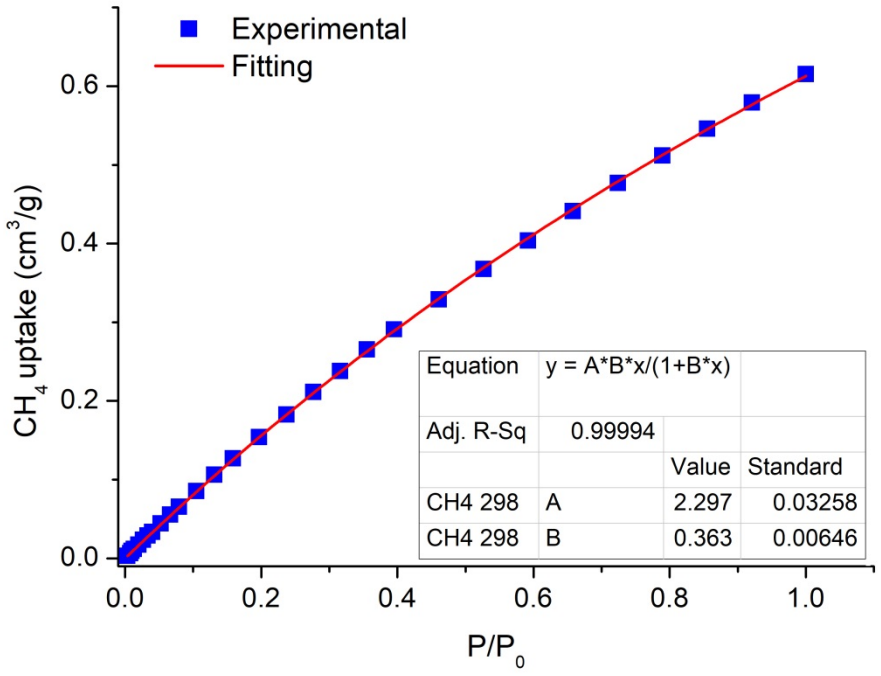

Figure S18. Single-site Langmuir fitting of CH_4 adsorption of **CPM-74** at 298 K.

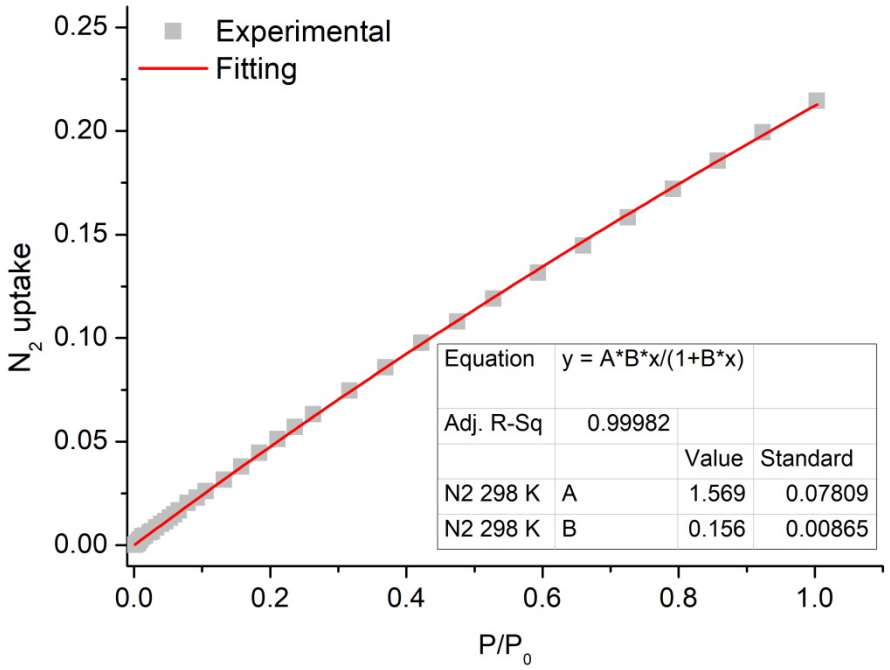

Figure S19. Single-site Langmuir fitting of N_2 adsorption of **CPM-74** at 298 K.

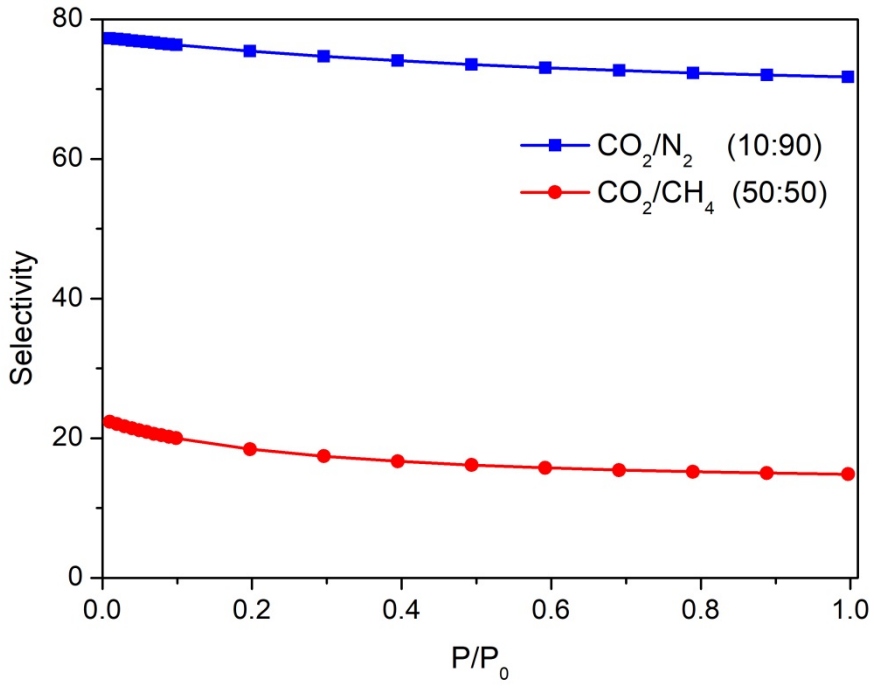

Figure S20. Adsorption selectivity predicted by IAST of **CPM-74** for CO_2/CH_4 (50%:50%) and CO_2/N_2 (10%:90%)

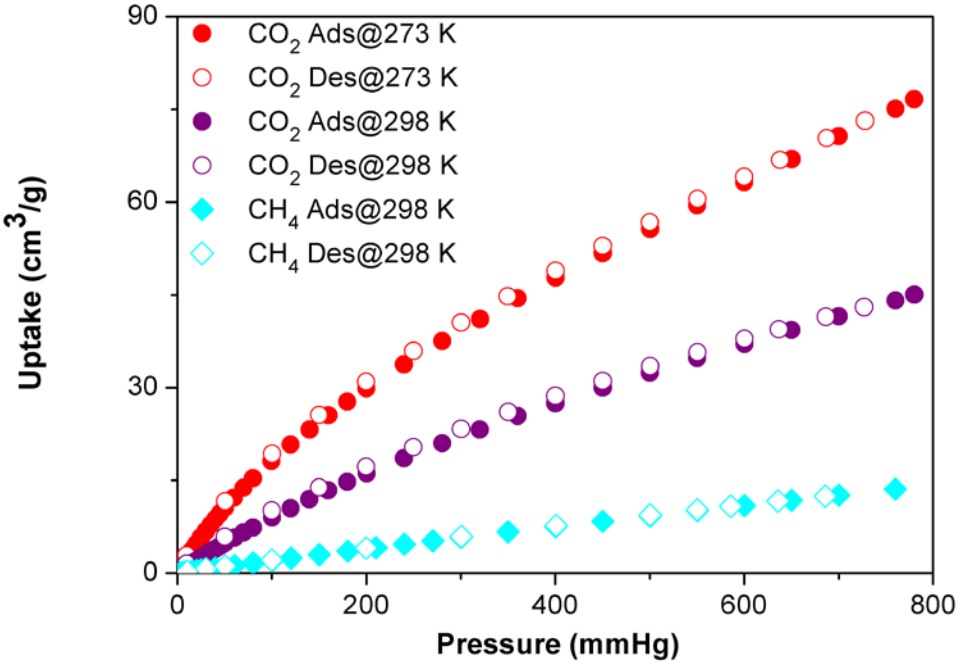

Figure S21. CO_2 and CH_4 adsorption isotherms of **CPM-75**.

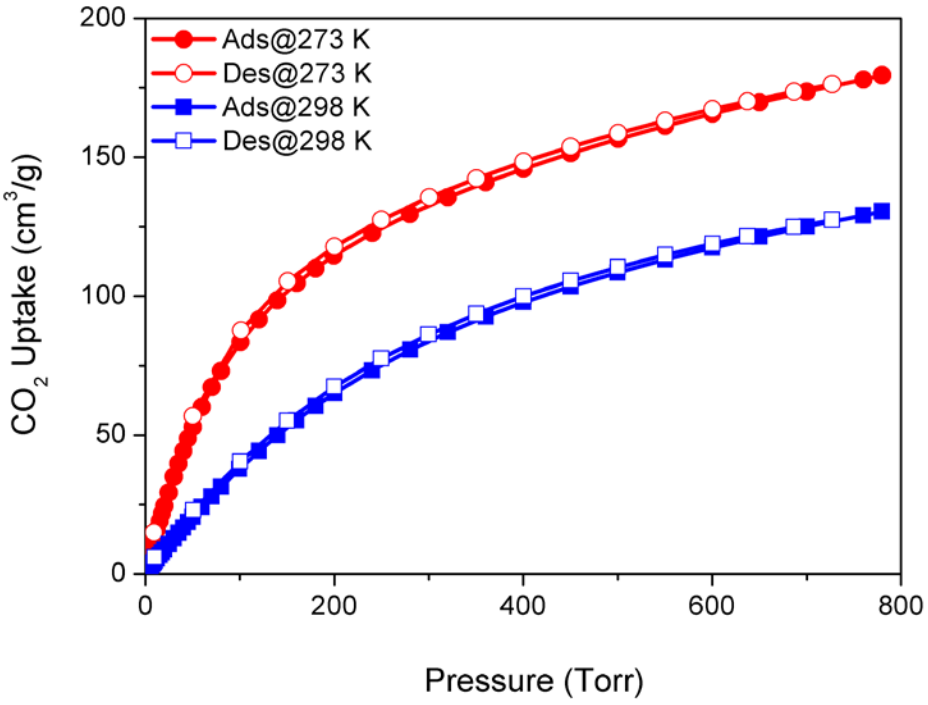

Figure S22. CO_2 adsorption isotherms of **MOF-74**.

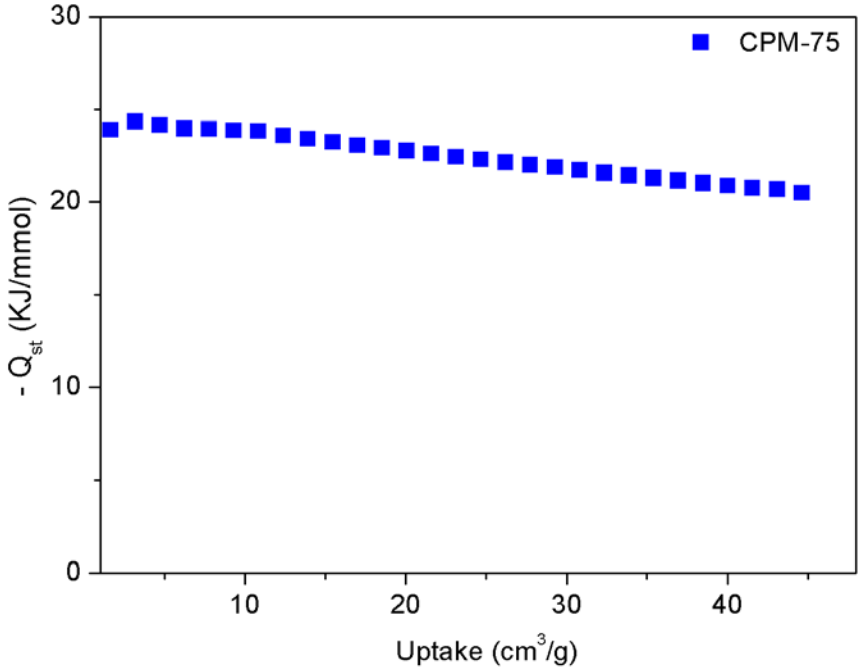

Figure S23. Heat of adsorption for CO_2 adsorption of CPM-75.

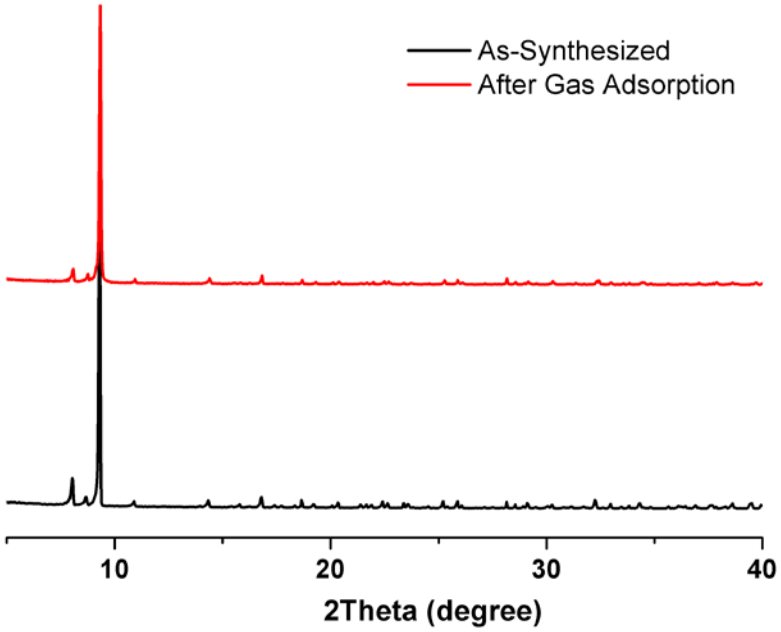

Figure S24. PXRD patterns of the ay-synthesized **CPM-74** and **CPM-74** after gas adsorption.

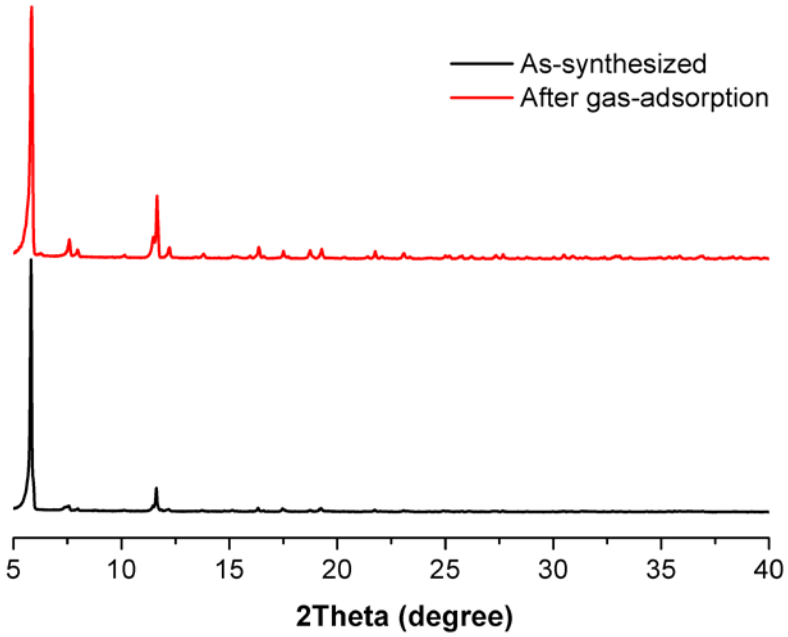

Figure S25. PXRD patterns of the ay-synthesized **CPM-75** and **CPM-75** after gas adsorption.

References:

[1] a) S. R. Caskey; A. G. Wong-Foy, A. J. Matzger. *J. Am. Chem. Soc.*, **2008**, *130*, 10870-10871; b) J. L. C. Rowsell, O. M. Yaghi. *J. Am. Chem. Soc*, **2006**, *128*, 1304-1315.

[2] A. L. Myers, J. M. Prausnitz. *AlChE J.*, **1965**, *11*, 121-127.

[3] Delley, B. From molecules to solids with the DMol 3 approach. *J. Chem. Phys.* **2000**, *113*, 7756.

[4] Grimme, S. *J. Comput. Chem.* **2006**, *27*, 1787.

[5] Grimme, S. Semiempirical Gga-Type Density Functional Constructed with a Long-Range Dispersion Correction. *J. Comput. Chem.* **2006**, *27*, 1787−1799.